LETTER

doi:10.1038/nature11493

Delayed build-up of Arctic ice sheets during 400,000-year minima in insolation variability

Qingzhen Hao[1], Luo Wang[1], Frank Oldfield[2], Shuzhen Peng[3], Li Qin[4], Yang Song[1,5], Bing Xu[1], Yansong Qiao[6], Jan Bloemendal[2] & Zhengtang Guo[1]

Knowledge of the past variability of climate at high northern latitudes during astronomical analogues of the present interglacial[1] may help to inform our understanding of future climate change. Unfortunately, long-term continuous records of ice-sheet variability in the Northern Hemisphere only are scarce because records of benthic ^{18}O content represent an integrated signal of changes in ice volume in both polar regions[2]. However, variations in Northern Hemisphere ice sheets influence the Siberian High[3] (an atmospheric pressure system), so variations in the East Asian winter monsoon (EAWM)—as recorded in the aeolian dust deposits on the Chinese Loess Plateau—can serve as a useful proxy of Arctic climate variability before the ice-core record begins. Here we present an EAWM proxy record using grain-size variations in two parallel loess sections representative of sequences across the whole of the Chinese Loess Plateau over the past 900,000 years. The results show that during periods of low eccentricity and precessional variability at approximately 400,000-year intervals, the grain-size-inferred intensity of the EAWM remains weak for up to 20,000 years after the end of the interglacial episode of high summer monsoon activity and strong pedogenesis. In contrast, there is a rapid increase in the EAWM after the end of most other interglacials. We conclude that, for both the 400,000-year interglacials, the weak EAWM winds maintain a mild, non-glacial climate at high northern latitudes for much longer than expected from the conventional loess and marine oxygen isotope records. During these times, the less-severe summer insolation minima at 65° N (ref. 4) would have suppressed ice and snow accumulation, leading to a weak Siberian High and, consequently, weak EAWM winds.

Knowledge of natural climate variability at high northern latitudes is crucial for understanding the future development of the Northern Hemisphere ice sheets, the melting or growth of which would lead to major changes in sea level[5]. Key proxies for past glacial variability include ice-rafted debris and $\delta^{18}O$ in foraminifera preserved in marine sediments. The $\delta^{18}O$ records, frequently used as a measure of changes in ice volume, actually reflect variability in both polar regions[2], and may also be overprinted by deep-water temperature variability[6]. Direct sedimentary records of Northern Hemisphere polar ice sheets exist only for the late Quaternary period, and longer-term records are scarce[7].

EAWM variability is tightly linked to variations in high-northern-latitude climate via the Siberian High[3] (Fig. 1, Supplementary Fig. 1 and Supplementary Information). This allows the use of the loess record of the last 900,000 years (900 kyr) from the Chinese Loess Plateau (CLP) to show the timing of build-up of Northern Hemisphere ice sheets around the 413-kyr minima in eccentricity and precessional variability. This time frame falls within the current period of dominantly eccentricity-paced glacial–interglacial cycles and has also provided the most comprehensive records of climate change over the CLP in terms of both temporal resolution and spatial coverage (Supplementary Figs 2–4).

Orbital changes in summer insolation at high northern latitudes drive the sequence of glacial–interglacial alternations that have characterized the Quaternary Epoch. We live in a time of low-amplitude precessional insolation variability modulated by the 413-kyr eccentricity cycle. The closest, relatively recent, analogues for the present interglacial occur around marine oxygen isotope stages 11 and 19 (MIS 11 and MIS 19; ref. 1). Despite recent efforts to reconcile them, there remain significant discrepancies in estimates of the length of MIS 11 (for example), both between model-based inferences[1,8] and reconstructions from geological records[9–11] and among the geologically based estimates themselves[9–13]. This work adds independent, empirically based data from Northern Hemisphere terrestrial archives not previously used to estimate MIS lengths.

The loess–palaeosol sequences in the CLP comprise high-resolution archives of East Asian monsoon climate variability[3,14–16]. The climate in this region is mainly controlled by two seasonally alternating monsoon circulations, the warm/humid southerly East Asian summer monsoon (EASM) and the dry/cold northerly EAWM. The EAWM refers to the movement of cold air over Asia coming from the Siberian High mainly in response to strong and continuous radiative cooling in the lower troposphere over snow-covered surfaces[17]. The predominance of low-altitude EAWM winds in transporting the dust deposited on the CLP is

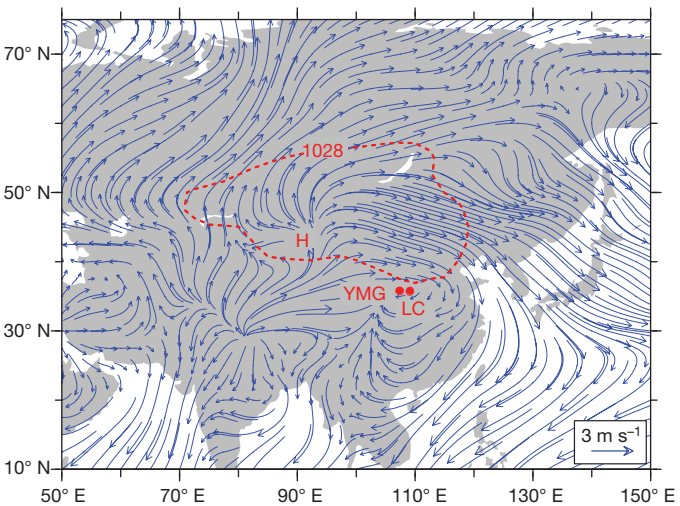

Figure 1 | Location map with the surface circulation over Eurasia in winter. Dec–Jan–Feb mean surface vector winds (blue arrows) based on the NCEP-DOE Reanalysis 2 data during 1979–2011 at http://www.esrl.noaa.gov/psd/data/gridded/reanalysis/. The grey area indicates land. 'H' indicates the centre of the Siberian High, and the area enclosed by the red-dashed line shows the region with mean sea level pressure exceeding 1,028 hPa. 'YMG' and 'LC' refer to the Yimaguan and Luochuan loess sections in this work.

[1]Key Laboratory of Cenozoic Geology and Environment, Institute of Geology and Geophysics, Chinese Academy of Sciences, PO Box 9825, Beijing 100029, China. [2]School of Environmental Sciences, University of Liverpool, Liverpool L69 7ZT, UK. [3]Key Laboratory of Tourism and Resources Environment in Universities of Shandong, Taishan University, Taian 271021, China. [4]Chongqing Three Gorges Institute of Paleoanthropology, China Three Gorges Museum, Chongqing 400015, China. [5]Graduate University of Chinese Academy of Sciences, Beijing 100049, China. [6]Institute of Geomechanics, Chinese Academy of Geological Sciences, Beijing 100081, China.

clearly indicated by an approximately north–south gradient of decreasing loess grain size[18].

The two loess–palaeosol sections used here, Yimaguan (35° 55′ N, 107° 37′ E) and Luochuan (35° 43′ N, 109° 25′ E), preserve a relatively complete suite of mineral dust deposits and can be well correlated by distinctive stratigraphic markers[19,20]. The chronology of the Yimaguan and Luochuan loess sections was generated by correlation of the studied sequences with the benthic $\delta^{18}O$ stack LR04 (ref. 10) (see Methods Summary).

Magnetic susceptibility and grain size are two well accepted proxies for summer and winter monsoon climates, respectively[3,14,15,21]. Justification for their use and their close correlation with other, independent proxies is provided in the Supplementary Figs 1 and 5, and related discussion. Here, the time series of the EAWM and EASM was reconstructed using the content of particles over 32 μm in size (GT32) and frequency-dependent magnetic susceptibility (χ_{fd}) of bulk samples from the two sections. The samples were usually analysed at 5-cm intervals for both sections, with 2.5-cm intervals for palaeosols S1 (12.875–16.100 m depth) and S5 (53.075–59.825 m depth) from Yimaguan. The 5-cm interval represents an average time resolution for loess and palaeosol layers of 0.36 kyr and 0.89 kyr for Yimaguan, and 0.56 kyr and 1.24 kyr for Luochuan.

The temporal changes in GT32 and χ_{fd} can be closely correlated between the two sections (Fig. 2d–g). During glacial times, high GT32 and minimum χ_{fd} values indicate that the climate on the CLP was characterized by overall strong EAWM winds and weakened EASM winds. Here, as reported in previous studies[21,22], the climate during interglacial times was characterized by much weaker EAWM winds and strengthened EASM winds. The GT32 time series shows orbital periodicities of 41 kyr and 23 kyr; the χ_{fd} time series shows orbital periodicities of 100 kyr, 41 kyr and 23 kyr (Supplementary Fig. 9), confirming the pacing of the changes by variations in the Earth's orbit.

Comparison between the EAWM and EASM proxy records (Fig. 2d–g) reveals major differences in the amplitude of fluctuation in glacial periods between the two monsoon climate components. The summer monsoon is very weak overall in the glacial periods, with the χ_{fd} curves in Fig. 2e and g nearly parallel to the marine $\delta^{18}O$ record (Fig. 2c). However, as found in previous studies[21,22], the winter monsoon has strong precessional cycles in several glacial loess units, such as L2, L5 and L6. These precession cycles match well with those predicted by the theoretical model of ice volume in the Northern Hemisphere[23] (Fig. 2b). The contrast in precessional cycles between summer and winter monsoon proxies highlights the fact that they have evolved in a relatively independent manner and are controlled by different driving factors. The grain-size records in loess lack the 'saw-tooth' shape typical of the marine $\delta^{18}O$ curve, implying that factors other than Northern Hemisphere ice volume have affected grain-size variations during glacial intervals. However, on orbital timescales, the extent of Northern Hemisphere ice sheets plays the leading role in controlling changes in loess grain size, hence our use here of these changes to indicate the large-scale growth of Northern Hemisphere ice sheets.

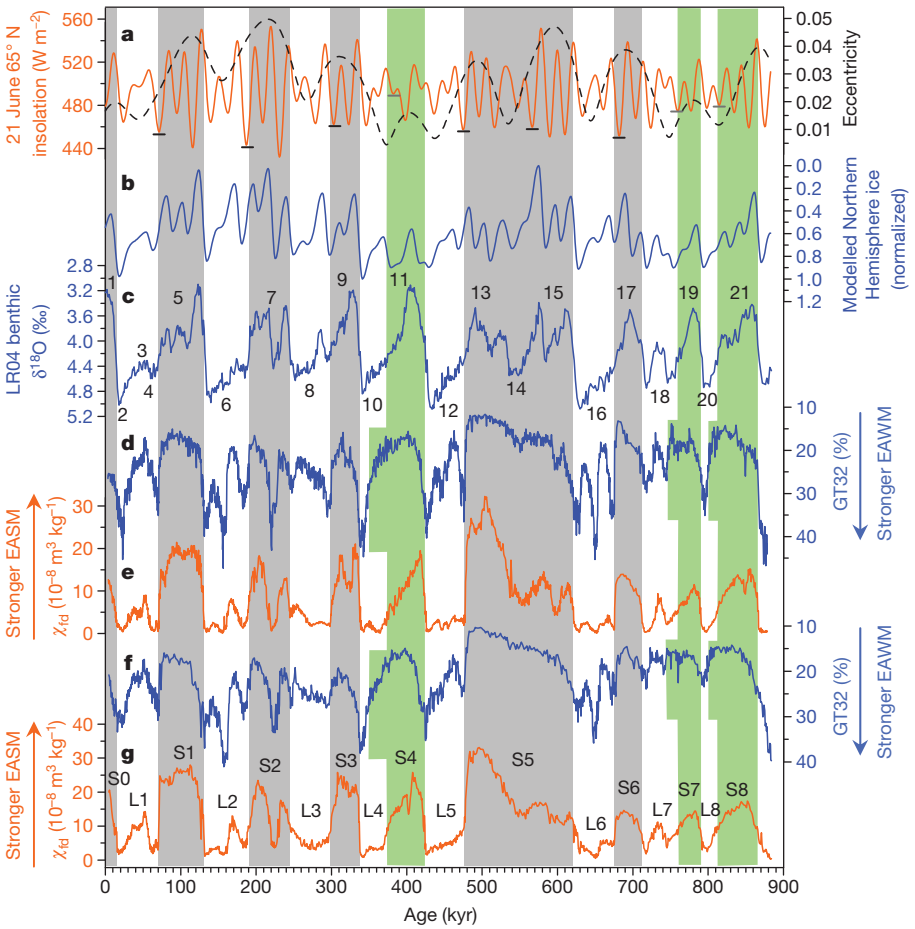

Figure 2 | Comparison of the East Asian winter monsoon (EAWM) and summer monsoon (EASM) proxy records in loess with other palaeoclimatic data of the past 880 kyr. **a**, 21 June insolation 65° N (orange trace)and long-term variations of eccentricity[4] (black trace). Short black (or grey) horizontal bars mark the strong (or weak) insolation minima coincident with each glacial inception. **b**, Northern Hemisphere modelled ice volume[23]. **c**, Benthic $\delta^{18}O$ stack LR04 (ref. 10). Numbers indicate MIS. **d**, Grain-size data expressed as GT32 (>32-μm particle content) in the Yimaguan loess section. **e**, Frequency-dependent magnetic susceptibility (χ_{fd}) in the Yimaguan loess section. **f** and **g**, GT32 and χ_{fd} data in the Luochuan loess section, respectively. The major loess and palaeosol units are labelled. The shaded areas indicate the major palaeosol units and their correlation with other palaeoclimatic records, with the green shading highlighting the delayed changes in loess grain size.

The most striking feature in the proxy records is that there are two types of coupling between EAWM and EASM at interglacial–glacial transitions (Fig. 2d–g and Supplementary Fig. 11). For most interglacial-to-glacial transitions (palaeosol S1 to loess unit L1, S2–L2, S3–L3, S5–L5 and S6–L6), the increase in GT32 values coincides closely with the decrease in the χ_{fd} values, indicating that the increased wind strength of the EAWM and weakening of the EASM were synchronous. However, at the transition of MIS 11 to MIS 10 (S4–L4), there is a period of around 20 kyr during which fine-grained loess persists after χ_{fd} values have decreased to levels typical of glacial loess. Such decoupled changes can also be found at the boundaries of S7–L7 and S8–L8. The decoupling is independent of the chronology model (Supplementary Fig. 6 for loess proxies plotted against depth). Comparison with the record of summer insolation at 65° N (ref. 4 and Fig. 2a) indicates that these three exceptions occur around minima in insolation variability modulated by the 413-kyr eccentricity cycle.

The EAWM proxy records in this study reveal different histories of Northern Hemisphere ice-volume growth at the conclusion of different interglacial periods. The reduction in boreal summer insolation is thought to be the primary trigger for glaciation[24,25]. The alignment of obliquity and precession insolation minima is important because low obliquity plays a significant part in reinforcing the processes driving glacial inception[25,26]. The amplitude of summer insolation variability in the precessional band is modulated at the eccentricity periods of 100 kyr and 413 kyr. At times of high eccentricity, each glacial inception (MIS 16, MIS 12, MIS 8, MIS 6 and MIS 4) was triggered by a very low precessional minimum of summer insolation (Fig. 2a), favouring the rapid accumulation of snow/ice at high northern latitudes. When the high-northern-latitude climate began to experience glacial conditions, the presence of the ice sheets and lowered CO_2 would have made the northern continents persistent sources for cold air surges[27]. The consequently strong EAWM winds would have led to a cold and arid climate over the Eurasian region[27], and carried coarser aeolian dust to the CLP, reflecting both increased wind strength and a southward expansion of the zone of extreme aridity. Therefore, the rapidly strengthening EAWM in these glacial periods indicates rapid build-up of ice-sheets at high northern latitudes, consistent with the benthic $\delta^{18}O$ records (Fig. 2c).

At times of low eccentricity in the 413-kyr cycles, all three glacials after each of MIS 21, MIS 19 and MIS 11 (corresponding to palaeosols S8, S7 and S4) were triggered by a very weak precessional insolation minimum leading to warm summer conditions unfavourable to Northern Hemisphere ice-sheet build-up at the inception of each of MIS 20, MIS 18 and MIS 10 (Fig. 2a). The interval lacking coarse-grained loess in early MIS 10 (L4) appears to span a precessional cycle and this is in sharp contrast to the records during high eccentricity periods in the 413-kyr cycle (Fig. 3). The continuing fine-grained loess deposition spanning nearly 20 kyr indicates a weak EAWM comparable to that during the MIS 11 interglacial (Figs 2 and 3). Owing to their inherent link with Northern Hemisphere ice extent, the weak EAWM and Siberian High during early MIS 10 strongly suggest that the high-northern-latitude climate was still experiencing non-glacial conditions with limited ice-sheet extent. This is strongly supported by independent pollen records off southwest Greenland that indicate a nearly ice-free Greenland during the MIS 11 optimum and a prolonged temperate climate for around 360 kyr (ref. 7). There are similar indications for the early glacial period recorded above palaeosols S7 (MIS 19) and S8 (MIS 21) (Fig. 2 and Supplementary Fig. 12).

Although the EAWM proxy records indicate a prolonged non-glacial climate at high northern latitudes, the χ_{fd} indicates that the summer monsoon significantly weakened after the end of the three exceptional interglacials: MIS 21, MIS 19 and MIS 11. The CLP is located on the fringe of the EASM, which becomes displaced over hundreds of kilometres in a north–south direction during glacial–interglacial cycles[16]. The displacement of the summer monsoon climate regime reflects, among other factors, distance from the sea. The sea level history extending to 500 kyr BP (before present) shows that sea level decreased gradually

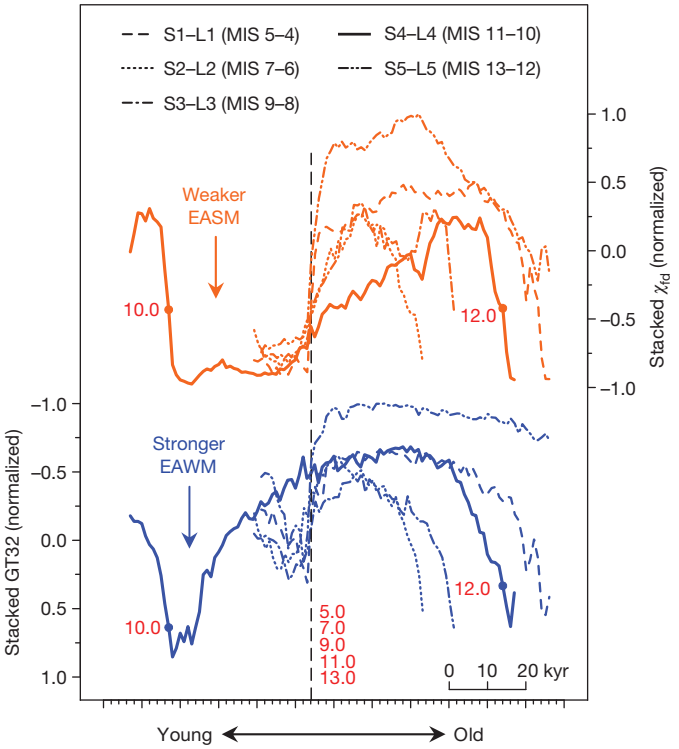

Figure 3 | Comparison of the stacked loess records of East Asian monsoon climate around the last five interglacial–glacial transitions. The grain size, GT32, and frequency-dependent magnetic susceptibility, χ_{fd}, data in different interglacial–glacial transitions are aligned (vertical dashed line) using the termination age of each interglacial defined by the benthic $\delta^{18}O$ stack LR04 (ref. 10), and are plotted against the uniform time-length unit. Numbers indicate MIS boundaries (red text). The stacked records are generated by averaging normalized GT32 and χ_{fd}, respectively. The normalized data were first interpolated linearly at 1-kyr intervals before stacking.

during early MIS 10 (ref. 28). This would have placed the CLP beyond the control of the EASM by increasing the distance from the source of moisture[16]. We suggest that the changes in sea level and $\delta^{18}O$ may have

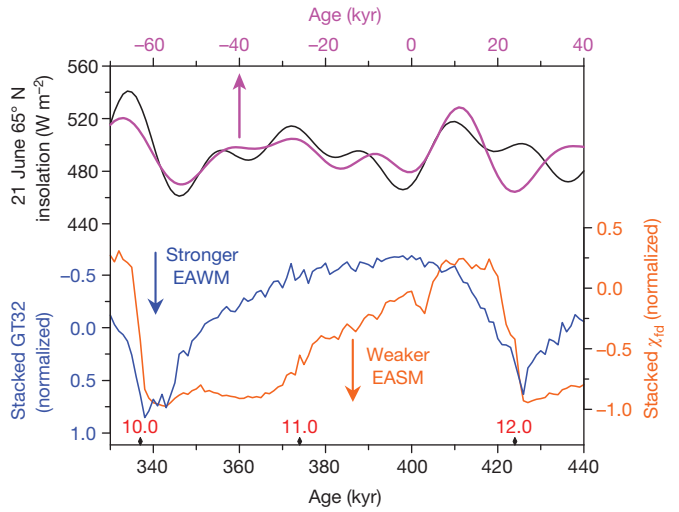

Figure 4 | Summer insolation during MIS 11–10 compared with present and future summer insolation. MIS 11 is selected as an astronomical analogue based on the high linear correlation of 65° N insolation in June between periods of 405–340 kyr BP and of 5 kyr BP to 60 kyr after present (AP)[1]. Only the insolation of 40 kyr BP–70 kyr AP, shown as a purple line, is plotted against the upper *x* axis (negative age refers to the future). MIS numbering (in red) is given along the bottom *x* axis.

been caused by a build-up of ice volume in the Antarctic region during early MIS 10 (Supplementary Fig. 13). Asymmetrical development of hemispheric ice sheets has been suggested by climate models[29].

Astronomically driven insolation during the present interglacial and in the near future is characterized by its low-amplitude variability. The best analogue is MIS 11 (ref. 1), though future 23-kyr precessional variability is even weaker than it was across the MIS 11–MIS 10 transition (Fig. 4). In terms of orbital forcing, the closest comparison for the present day is with conditions around 400 kyr BP, some 40–45 kyr before evidence for the onset of glacial conditions in the Arctic. These observations lead us to speculate that the future Arctic climate may still remain in non-glacial mode for more than 40 kyr (approximately two precessional cycles), even without taking into account forcing by the rapid increase in anthropogenically generated greenhouse gases.

METHODS SUMMARY

Grain-size analysis. After removal of organic matter by 10% H_2O_2, of carbonate by 10% HCl, and dispersal using 0.05 N $(NaPO_3)_6$, samples were measured using a Mastersizer 2000 analyser with size range of 0.02–2,000 μm in diameter and with a precision of ±1%. The GT32 (>32-μm particle content) used here shows good correlation with median grain-size changes (Supplementary Fig. 6).

Magnetic susceptibility. Low-frequency magnetic susceptibility (χ_{lf}) and high-frequency magnetic susceptibility (χ_{hf}) were measured at 0.47 kHz and 4.7 kHz, respectively, using a Bartington Instruments MS 2B magnetic susceptibility meter. Frequency-dependent susceptibility, χ_{fd}—the difference between χ_{lf} and χ_{hf}—is an indicator of the formation of fine-grained secondary ferrimagnetic oxides as a result of pedogenesis[30], and is closely linked with the strength of the summer monsoon. It is a better indicator of pedogenesis than χ_{lf}, which includes signals from both fine pedogenic particles and coarse detrital aeolian input.

Establishment of the chronology. The chronology of the Yimaguan and Luochuan loess sections was established using the accepted correlation scheme between Chinese loess and deep-sea sediments[21,22] (Supplementary Figs 7–10). The absolute age control points are transferred from MIS boundaries[10] by correlating them with interglacial palaeosol boundaries[19,20]. Between control points, interpolation, weighted by grain-size[15], was used to generate the timescale. The age uncertainties arising from choice of age control points and interpolation methods are averaged to within a few thousand years (Supplementary Fig. 7). Therefore, the duration of delayed changes in grain size is much greater than age uncertainties. The cross-spectral analysis with the theoretical orbital record[4] of the Earth confirms the validity of the present chronology (Supplementary Fig. 9).

Received 7 April; accepted 7 August 2012.
Published online 3 October 2012.

1. Loutre, M. F. & Berger, A. Marine Isotope Stage 11 as an analogue for the present interglacial. *Global Planet. Change* **36,** 209–217 (2003).
2. Raymo, M. E., Lisiecki, L. E. & Nisancioglu, K. H. Plio-Pleistocene ice volume, Antarctic climate, and the global $\delta^{18}O$ record. *Science* **313,** 492–495 (2006).
3. Ding, Z., Liu, T., Yu, Z., Guo, Z. & Zhu, R. Ice-volume forcing of East Asian winter monsoon variations in the past 800,000 years. *Quat. Res.* **44,** 149–159 (1995).
4. Laskar, J., Joutel, F. & Boudin, F. Orbital, precessional, and insolation quantities for the Earth from -20 Myr to +10 Myr. *Astron. Astrophys.* **270,** 522–533 (1993).
5. Alley, R. B., Clark, P. U., Huybrechts, P. & Joughin, I. Ice-sheet and sea-level changes. *Science* **310,** 456–460 (2005).
6. Shackleton, N. J. The 100,000-year ice-age cycle identified and found to lag temperature, carbon dioxide, and orbital eccentricity. *Science* **289,** 1897–1902 (2000).
7. de Vernal, A. & Hillaire-Marcel, C. Natural variability of Greenland climate, vegetation, and ice volume during the past million years. *Science* **320,** 1622–1625 (2008).
8. Berger, A. & Loutre, M. F. An exceptionally long interglacial ahead? *Science* **297,** 1287–1288 (2002).
9. McManus, J. F., Oppo, D. W. & Cullen, J. L. A 0.5-million-year record of millennial-scale climate variability in the North Atlantic. *Science* **283,** 971–975 (1999).
10. Lisiecki, L. & Raymo, M. A Pliocene-Pleistocene stack of 57 globally distributed benthic $\delta^{18}O$ records. *Paleoceanography* **20,** PA1003 (2005).
11. Jouzel, J. *et al.* Orbital and millennial Antarctic climate variability over the past 800,000 years. *Science* **317,** 793–796 (2007).
12. Howard, W. R. A warm future in the past. *Nature* **388,** 418–419 (1997).
13. Droxler, A. W., Alley, R. B., Howard, W. R., Poore, R. Z. & Burckle, L. H. in *Earth's Climate and Orbital Eccentricity: The Marine Isotope Stage 11 Question* (eds Droxler, A. W., Poore, R. Z. & Burckle, L. H.) 1–14 (AGU Geophys. Monogr. Ser. 137, 2003).
14. An, Z. *et al.* The long-term paleomonsoon variation recorded by the loess-paleosol sequence in central China. *Quat. Int.* **7–8,** 91–95 (1990).
15. Porter, S. C. & An, Z. S. Correlation between climate events in the North Atlantic and China during last glaciation. *Nature* **375,** 305–308 (1995).
16. Liu, T. & Ding, Z. Chinese loess and the paleomonsoon. *Annu. Rev. Earth Planet. Sci.* **26,** 111–145 (1998).
17. Panagiotopoulos, F., Shahgedanova, M., Hannachi, A. & Stephenson, D. B. Observed trends and teleconnections of the Siberian high: a recently declining center of action. *J. Clim.* **18,** 1411–1422 (2005).
18. Nugteren, G. & Vandenberghe, J. Spatial climatic variability on the Central Loess Plateau (China) as recorded by grain size for the last 250 kyr. *Global Planet. Change* **41,** 185–206 (2004).
19. Liu, T. *Loess and the Environment* (China Ocean, 1985).
20. Kukla, G. & An, Z. S. Loess stratigraphy in central China. *Palaeogeogr. Palaeoclimatol. Palaeoecol.* **72,** 203–225 (1989).
21. Sun, Y., Clemens, S. C., An, Z. & Yu, Z. Astronomical timescale and palaeoclimatic implication of stacked 3.6-Myr monsoon records from the Chinese Loess Plateau. *Quat. Sci. Rev.* **25,** 33–48 (2006).
22. Ding, Z. L. *et al.* Stacked 2.6-Ma grain size record from the Chinese loess based on five sections and correlation with the deep-sea $\delta^{18}O$ record. *Paleoceanography* **17,** 1033 (2002).
23. Imbrie, J. & Imbrie, J. Z. Modeling the climatic response to orbital variations. *Science* **207,** 943–953 (1980).
24. Milankovitch, M. *Kanon der Erdebestrahlung und seine Anwendung auf das Eiszeitenproblem* (Stamparija Mihaila Curcica, 1941); *Canon of Insolation and the Ice-age Problem* [English transl.] (Israel Program for Scientific Translations, US Department of Commerce and the National Science Foundation, 1969).
25. Vettoretti, G. & Peltier, W. Sensitivity of glacial inception to orbital and greenhouse gas climate forcing. *Quat. Sci. Rev.* **23,** 499–519 (2004).
26. Ruddiman, W. F. Orbital insolation, ice volume, and greenhouse gases. *Quat. Sci. Rev.* **22,** 1597–1629 (2003).
27. Kutzbach, J. *et al.* Climate and biome simulations for the past 21,000 years. *Quat. Sci. Rev.* **17,** 473–506 (1998).
28. Rohling, E. *et al.* Antarctic temperature and global sea level closely coupled over the past five glacial cycles. *Nature Geosci.* **2,** 500–504 (2009).
29. Huybrechts, P. & de Wolde, J. The dynamic response of the Greenland and Antarctic ice sheets to multiple-century climatic warming. *J. Clim.* **12,** 2169–2188 (1999).
30. Zhou, L. P., Oldfield, F., Wintle, A. G., Robinson, S. G. & Wang, J. T. Partly pedogenic origin of magnetic variations in Chinese loess. *Nature* **346,** 737–739 (1990).

Supplementary Information is available in the online version of the paper.

Acknowledgements This work was supported by the National Natural Science Foundation of China (grant 41172323), Ministry of Science and Technology (grant 2010CB950204), Ministry of Land and Resources (grant 201211077), and the Chinese Academy of Sciences.

Author Contributions Q.H. and L.W. designed the study. Q.H. and Y.S. undertook the field work. S.P. and Q.H. organized and supervised the grain-size measurement. Y.S. and Q.H. performed the magnetic susceptibility measurements. Q.H. and F.O. wrote the manuscript. All the authors contributed to the interpretation of the data and provided significant input to the final manuscript.

Author Information Reprints and permissions information is available at www.nature.com/reprints. The authors declare no competing financial interests. Readers are welcome to comment on the online version of the paper. Correspondence and requests for materials should be addressed to Q.H. (haoqz@mail.iggcas.ac.cn) or F.O. (oldfield.f@gmail.com).